

Maximum principle for the finite element solution of time dependent anisotropic diffusion problems

Xianping Li ^{*} Weizhang Huang [†]

Preservation of the maximum principle is studied for the combination of the linear finite element method in space and the θ -method in time for solving time dependent anisotropic diffusion problems. It is shown that the numerical solution satisfies a discrete maximum principle when all element angles of the mesh measured in the metric specified by the inverse of the diffusion matrix are nonobtuse and the time step size is bounded below and above by bounds proportional essentially to the square of the maximal element diameter. The lower bound requirement can be removed when a lumped mass matrix is used. In two dimensions, the mesh and time step conditions can be replaced by weaker Delaunay-type conditions. Numerical results are presented to verify the theoretical findings.

AMS 2010 Mathematics Subject Classification. 65M60, 65M50

Key words. finite element, time dependent, anisotropic diffusion, maximum principle

1 Introduction

We are concerned with the linear finite element solution of the initial-boundary value problem (IBVP) of a linear diffusion equation,

$$\begin{cases} u_t - \nabla \cdot (\mathbb{D} \nabla u) = f(\mathbf{x}, t), & \text{in } \Omega_T = \Omega \times (0, T] \\ u(\mathbf{x}, t) = g(\mathbf{x}, t), & \text{on } \partial\Omega \times [0, T] \\ u(\mathbf{x}, 0) = u_0(\mathbf{x}), & \text{in } \Omega \times \{t = 0\} \end{cases} \quad (1)$$

where $\Omega \subset \mathbb{R}^d$ ($d \geq 1$) is a connected polygonal or polyhedral domain, $T > 0$ is a fixed time, $f(\mathbf{x}, t)$, $g(\mathbf{x}, t)$ and $u_0(\mathbf{x})$ are given functions, and \mathbb{D} is the diffusion matrix. We assume that $\mathbb{D} = \mathbb{D}(\mathbf{x})$ is a general symmetric and strictly positive definite matrix-valued function on Ω_T . It includes both isotropic and anisotropic diffusion as special examples. In the former case, \mathbb{D} takes the form $\alpha(\mathbf{x})I$, where I is the $d \times d$ identity matrix and $\alpha = \alpha(\mathbf{x})$ is a scalar function. In the latter case, on the other hand, \mathbb{D} has not-all-equal eigenvalues at least on a certain portion of Ω_T . Note that we consider only time independent \mathbb{D} in this work. In principle, the procedure used in this work can also apply to the time dependent situation. For that situation, however, different meshes are needed for different time

^{*}Department of Mathematics, the University of Central Arkansas, Conway, AR 72034, U.S.A. (XianpingL@uca.edu)

[†]Department of Mathematics, the University of Kansas, Lawrence, KS 66045, U.S.A. (huang@math.ku.edu)

steps and the numerical solution has to be interpolated between these meshes. Then, a conservative interpolation scheme must be employed in order for the underlying scheme to preserve the maximum principle, non-negativity, or monotonicity. The development of conservative interpolation schemes and their use for unstructured meshes is an interesting research topic in its own right (e.g., see [1]) and beyond the scope of the current study. To avoid this possible complexity, we restrict our attention to the time independent diffusion matrix in this work.

Anisotropic diffusion problems arise from various areas of science and engineering including plasma physics [2, 3, 4, 5, 6, 7], petroleum reservoir simulation [8, 9, 10, 11, 12], and image processing [13, 14, 15, 16, 17, 18]. IBVP (1) is a prototype of those anisotropic diffusion problems. It satisfies the maximum principle

$$\max_{(\mathbf{x},t) \in \overline{\Omega}_T} v(\mathbf{x},t) = \max \left\{ 0, \max_{(\mathbf{x},t) \in \partial\Omega_T} v(\mathbf{x},t) \right\}, \quad \forall v \text{ satisfying } v_t - \nabla \cdot (\mathbb{D}\nabla v) \leq 0 \text{ in } \Omega_T \quad (2)$$

where $\partial\Omega_T$ denotes the parabolic boundary (i.e., $\partial\Omega \times \{0 < t \leq T\} \cup \Omega \times \{t = 0\}$). When a standard numerical method such as a finite element or a finite difference method is used to solve this problem, the numerical solution may violate the maximum principle and contain spurious oscillations. It is of practical and theoretical importance to study when a numerical solution satisfies a discrete maximum principle (DMP) (cf. (40) in Sect. 3) as well as develop DMP-preserving numerical schemes.

The research topic has attracted considerable attention from researchers since 1970's and success has been made for elliptic diffusion problems; e.g. see [19, 20, 21, 22, 23, 24, 25, 26, 27, 28, 29, 30, 12, 31, 32, 33, 34, 35, 36]. For example, it is shown in [19, 21] that for isotropic diffusion problems, the requirement of all element angles of the mesh to be nonobtuse is sufficient for the linear finite element approximation to satisfy DMP. In two dimensions, this nonobtuse angle condition can be replaced by a weaker, so-called Delaunay condition [34] which requires the sum of any pair of angles facing a common interior edge to be less than or equal to π . For anisotropic diffusion problems, Drăgănescu et al. [22] show that the nonobtuse angle condition fails to guarantee DMP satisfaction for a linear finite element approximation. Various techniques have been proposed to reduce spurious oscillations, including local matrix modification [26, 29], mesh optimization [12], and mesh adaptation [28]. An anisotropic nonobtuse angle condition, which uses element angles measured in the metric specified by \mathbb{D}^{-1} instead of angles measured in the Euclidean metric (as in the nonobtuse angle condition), is developed in [27] to guarantee DMP satisfaction for anisotropic diffusion problems. A weaker, Delaunay-type mesh condition is obtained in [23] for two-dimensional problems. The results of [23, 27] are extended in [30] to problems containing convection and reaction terms.

On the other hand, less progress has been made for time-dependent problems; e.g., see [37, 38, 39, 40, 41, 42, 43, 44, 45, 46, 47, 6, 48, 49, 50]. Most of the existing research has focused on isotropic diffusion problems. For example, Fujii [44] considers the heat equation and shows that the time step size should be bounded from below and above for a linear finite element approximation to satisfy DMP when the mesh satisfies the nonobtuse angle condition. He also shows that the lower bound requirement can be removed when a lumped mass matrix is used. The study is extended in [38] to a more general isotropic diffusion problem with a reaction term. Thomée and Wahlbin [48] consider general anisotropic diffusion problems and show that a semi-discrete conventional finite element solution does not satisfy DMP in general. Slope limiters are employed in [6] to improve DMP satisfaction for anisotropic thermal conduction in magnetized plasmas. Nonlinear finite volume methods are developed by Le Potier [51, 52] for time dependent problems.

The objective of this paper is to investigate conditions for the finite element approximation of IBVP (1) to satisfy DMP for a general diffusion matrix function. We are particularly interested in lower

and upper bounds on the time step size when the θ -method and the conventional linear finite element method are used for temporal and spatial discretization, respectively. Two types of simplicial mesh are considered, meshes satisfying the anisotropic nonobtuse angle condition [27] or a Delaunay-type mesh condition [23]. It is known that those meshes lead to DMP-satisfaction linear finite element approximations to steady-state anisotropic diffusion problems. A lumped mass matrix is also studied. The results obtained in this paper can be viewed as a generalization of Fujii's [44] to anisotropic diffusion problems although such generalization is not trivial.

The outline of this paper is as follows. In Sect. 2, the linear finite element solution of IBVP (1) is described. Sect. 3 is devoted to the development of DMP-satisfaction conditions. Numerical examples are presented in Sect. 4 to verify the theoretical findings. Finally, Sect. 5 contains conclusions.

2 Linear finite element formulation

Consider the linear finite element solution of IBVP (1). Assume that an affine family of simplicial triangulations $\{\mathcal{T}_h\}$ is given for the physical domain Ω . Define

$$U_g = \{v \in H^1(\Omega) \mid v|_{\partial\Omega} = g\}.$$

Denote the linear finite element space associated with mesh \mathcal{T}_h by U_g^h . A linear finite element solution $u^h(t) \in U_g^h$ for $t \in (0, T]$ to IBVP (1) is defined by

$$\int_{\Omega} \frac{\partial u^h}{\partial t} v^h d\mathbf{x} + \int_{\Omega} (\nabla v^h)^T \mathbb{D} \nabla u^h d\mathbf{x} = \int_{\Omega} f v^h d\mathbf{x}, \quad \forall v^h \in U_0^h \quad (3)$$

where $U_0^h = U_g^h$ with $g = 0$. This equation can be rewritten as

$$\sum_{K \in \mathcal{T}_h} \int_K \frac{\partial u^h}{\partial t} v^h d\mathbf{x} + \sum_{K \in \mathcal{T}_h} |K| (\nabla v^h)^T \mathbb{D}_K \nabla u^h d\mathbf{x} = \sum_{K \in \mathcal{T}_h} \int_K f v^h d\mathbf{x}, \quad \forall v^h \in U_0^h \quad (4)$$

where $|K|$ is the volume of element K and

$$\mathbb{D}_K = \frac{1}{|K|} \int_K \mathbb{D} d\mathbf{x}.$$

Equation (4) can be expressed in a matrix form. Denote the numbers of the elements, vertices, and interior vertices of \mathcal{T}_h by N_e , N_v , and N_{vi} , respectively. Assume that the vertices are ordered in such a way that the first N_{vi} vertices are the interior vertices. Then U_0^h and u^h can be expressed as

$$\begin{aligned} U_0^h &= \text{span}\{\phi_1, \dots, \phi_{N_{vi}}\}, \\ u^h &= \sum_{j=1}^{N_{vi}} u_j \phi_j + \sum_{j=N_{vi}+1}^{N_v} u_j \phi_j, \end{aligned} \quad (5)$$

where ϕ_j is the linear basis function associated with the j^{th} vertex, \mathbf{a}_j . We approximate the boundary and initial conditions in (1) as

$$u_j(t) = g_j \equiv g(\mathbf{a}_j, t), \quad j = N_{vi} + 1, \dots, N_v \quad (6)$$

$$u_j(0) = u_0(\mathbf{a}_j), \quad j = 1, \dots, N_v. \quad (7)$$

Substituting (5) into (4), taking $v^h = \phi_i$ ($i = 1, \dots, N_{vi}$), and combining the resulting equations with (6), we obtain the linear algebraic system

$$M \frac{d\mathbf{u}}{dt} + A \mathbf{u} = \mathbf{f}, \quad (8)$$

where $\mathbf{u} = (u_1, \dots, u_{N_{vi}}, u_{N_{vi}+1}, \dots, u_{N_v})^T$, $\mathbf{f} = (f_1, \dots, f_{N_{vi}}, g_{N_{vi}+1}, \dots, g_{N_v})^T$,

$$M = \begin{bmatrix} M_{11} & M_{12} \\ 0 & 0 \end{bmatrix}, \quad A = \begin{bmatrix} A_{11} & A_{12} \\ 0 & I \end{bmatrix}, \quad (9)$$

and I is the identity matrix of size $(N_v - N_{vi})$. The entries of mass matrix M , stiffness matrix A , and right-hand-side vector \mathbf{f} are given by

$$m_{ij} = \sum_{K \in \mathcal{T}_h} \int_K \phi_j \phi_i d\mathbf{x}, \quad i = 1, \dots, N_{vi}, \quad j = 1, \dots, N_v \quad (10)$$

$$a_{ij} = \sum_{K \in \mathcal{T}_h} |K| (\nabla \phi_i)^T \mathbb{D}_K \nabla \phi_j, \quad i = 1, \dots, N_{vi}, \quad j = 1, \dots, N_v \quad (11)$$

$$f_i = \sum_{K \in \mathcal{T}_h} \int_K f \phi_i d\mathbf{x}, \quad i = 1, \dots, N_{vi}. \quad (12)$$

We use the θ -method with a constant time step Δt for time integration. Let \mathbf{u}^n and \mathbf{u}^{n+1} be the computed solutions at the current and next time steps, respectively. Applying the θ -method to the first N_{vi} equations, we get

$$[M_{11} \ M_{12}] \frac{\mathbf{u}^{n+1} - \mathbf{u}^n}{\Delta t} + [A_{11} \ A_{12}] ((1 - \theta)\mathbf{u}^n + \theta\mathbf{u}^{n+1}) = \tilde{\mathbf{f}}^{n+\theta}, \quad (13)$$

where

$$\tilde{\mathbf{f}}^{n+\theta} = [f_1(t_n + \theta\Delta t), \dots, f_{N_{vi}}(t_n + \theta\Delta t)]^T.$$

For the last $N_v - N_{vi}$ equations (corresponding to the boundary condition), we use

$$u_j^{n+1} = g(\mathbf{a}_j, t_{n+1}), \quad j = N_{vi} + 1, \dots, N_v. \quad (14)$$

Combining (13) and (14), we have

$$B \mathbf{u}^{n+1} = C \mathbf{u}^n + \Delta t \mathbf{f}^{n+\theta}, \quad (15)$$

where

$$B = \begin{bmatrix} M_{11} & M_{12} \\ 0 & I \end{bmatrix} + \theta\Delta t \begin{bmatrix} A_{11} & A_{12} \\ 0 & 0 \end{bmatrix}, \quad (16)$$

$$C = \begin{bmatrix} M_{11} & M_{12} \\ 0 & 0 \end{bmatrix} - (1 - \theta)\Delta t \begin{bmatrix} A_{11} & A_{12} \\ 0 & 0 \end{bmatrix}, \quad (17)$$

$$\mathbf{f}^{n+\theta} = \left(f_1(t_n + \theta\Delta t), \dots, f_{N_{vi}}(t_n + \theta\Delta t), \frac{1}{\Delta t} g(\mathbf{a}_{N_{vi}+1}, t_{n+1}) \dots, \frac{1}{\Delta t} g(\mathbf{a}_{N_v}, t_{n+1}) \right)^T, \quad (18)$$

$$\mathbf{u}^0 = \mathbf{u}_0 = (u_0(\mathbf{a}_1), \dots, u_0(\mathbf{a}_{N_v}))^T. \quad (19)$$

It is worth noting that the right-hand side vector, $\mathbf{f}^{n+\theta}$, is formed from the values of the right-hand side function $f(\mathbf{x}, t)$ and the boundary function $g(\mathbf{x}, t)$. We are interested in conditions under which the scheme satisfies DMP.

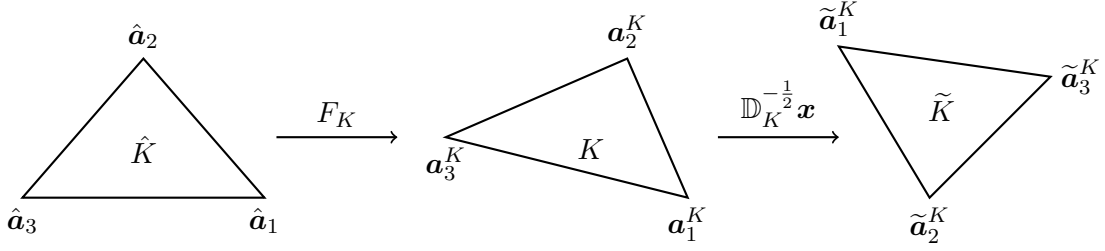


Figure 1: Sketch of coordinate transformations from \hat{K} to K and to \tilde{K} . Here, \hat{K} is the reference element and F_K is the affine mapping from \hat{K} to element K .

3 Conditions for DMP satisfaction

In this section we develop the conditions (on the mesh and time step size) under which scheme (15) satisfies DMP. The main tool is a result from [33] which states that the solution of a linear algebraic system satisfies DMP when the corresponding coefficient matrix is an M -matrix and has nonnegative row sums. We first discuss the general dimensional case along with the anisotropic nonobtuse angle condition developed in [27] and then study the two dimensional case with the Delaunay-type mesh condition developed in [23].

We introduce some notation. Consider a generic element $K \in \mathcal{T}_h$ and denote its vertices by $\mathbf{a}_1^K, \mathbf{a}_2^K, \dots, \mathbf{a}_{d+1}^K$. Denote the face opposite to vertex \mathbf{a}_i^K (i.e., the face not having \mathbf{a}_i^K as its vertex) by S_i^K and its unit inward (pointing to \mathbf{a}_i^K) normal by \mathbf{n}_i^K . The distance (or height) from vertex \mathbf{a}_i^K to face S_i^K is denoted by h_i^K . Define \mathbf{q} -vectors as

$$\mathbf{q}_i^K = \frac{\mathbf{n}_i^K}{h_i^K}, \quad i = 1, \dots, d+1. \quad (20)$$

Obviously, we have $h_i^K = 1/\|\mathbf{q}_i^K\|$.

We now consider the mapping $\mathbb{D}_K^{-\frac{1}{2}} \mathbf{x} : K \rightarrow \tilde{K}$; see Fig. 1. The \mathbf{q} -vectors and heights associated with \tilde{K} are denoted by $\tilde{\mathbf{q}}_i^K$, and \tilde{h}_i^K . We have relations

$$\tilde{\mathbf{a}}_i^K = \mathbb{D}_K^{-\frac{1}{2}} \mathbf{a}_i^K, \quad \tilde{S}_i^K = \mathbb{D}_K^{-\frac{1}{2}} S_i^K, \quad |\tilde{K}| = \det(\mathbb{D}_K)^{-\frac{1}{2}} |K|, \quad \tilde{\mathbf{q}}_i^K = \mathbb{D}_K^{\frac{1}{2}} \mathbf{q}_i^K, \quad \tilde{h}_i^K = \frac{1}{\|\tilde{\mathbf{q}}_i^K\|}. \quad (21)$$

The dihedral angle between surfaces \tilde{S}_i^K and \tilde{S}_j^K ($i \neq j$) is denoted by $\tilde{\alpha}_{ij}^K$. It can be expressed as

$$\cos(\tilde{\alpha}_{ij}^K) = -\frac{(\tilde{\mathbf{q}}_i^K)^T \tilde{\mathbf{q}}_j^K}{\|\tilde{\mathbf{q}}_i^K\| \cdot \|\tilde{\mathbf{q}}_j^K\|} = -\frac{(\mathbf{q}_i^K)^T \mathbb{D}_K \mathbf{q}_j^K}{\|\mathbf{q}_i^K\|_{\mathbb{D}_K} \|\mathbf{q}_j^K\|_{\mathbb{D}_K}}, \quad i \neq j \quad (22)$$

where $\|\mathbf{q}_i^K\|_{\mathbb{D}_K} = \sqrt{(\mathbf{q}_i^K)^T \mathbb{D}_K \mathbf{q}_i^K}$. Note that $\tilde{\alpha}_{ij}^K$ can be considered as a *dihedral angle of K measured in the metric specified by \mathbb{D}_K^{-1}* .

3.1 General dimensional case: $d \geq 1$

We now are ready for the development of the DMP satisfaction conditions for scheme (15) for the general dimensional case. We first have the following four lemmas.

Lemma 3.1. For any element $K \in \mathcal{T}_h$ and $i, j = 1, \dots, d+1$,

$$(\nabla\phi_i)^T \mathbb{D}_K \nabla\phi_j = \begin{cases} -\frac{\cos(\tilde{\alpha}_{ij}^K)}{\tilde{h}_i^K \tilde{h}_j^K}, & \text{for } i \neq j \\ \frac{1}{(\tilde{h}_i^K)^2}, & \text{for } i = j \end{cases} \quad (23)$$

where ϕ_i and ϕ_j are the linear basis functions associated with the vertices \mathbf{a}_i^K and \mathbf{a}_j^K , respectively. In two dimensions ($d = 2$),

$$|K|(\nabla\phi_i)^T \mathbb{D}_K \nabla\phi_j = -\frac{\sqrt{\det(\mathbb{D}_K)}}{2} \cot(\tilde{\alpha}_{ij}^K), \quad i \neq j, \quad i, j = 1, 2, 3. \quad (24)$$

Proof. see [23, 30]. \square

Lemma 3.2. The stiffness matrix A defined in (9) and (11) is an M -matrix and has nonnegative row sums if the mesh satisfies the anisotropic nonobtuse angle condition

$$0 < \tilde{\alpha}_{ij}^K \leq \frac{\pi}{2}, \quad \forall i, j = 1, \dots, d+1, i \neq j, \quad \forall K \in \mathcal{T}_h. \quad (25)$$

Proof. See [27, Theorem 2.1 and its proof]. \square

Lemma 3.3. Matrix B defined in (16) ($0 < \theta \leq 1$) is an M -matrix if the mesh satisfies (25) and the time step size satisfies

$$\Delta t \geq \frac{1}{\theta(d+1)(d+2)} \max_{K \in \mathcal{T}_h} \max_{\substack{i, j=1, \dots, d+1 \\ i \neq j}} \frac{h_i^K h_j^K}{\cos(\tilde{\alpha}_{ij}^K) \lambda_{\min}(\mathbb{D}_K)}. \quad (26)$$

Proof. We first show that $M + \theta\Delta t A$ is a Z -matrix, i.e., it has positive diagonal and nonpositive off-diagonal entries. From (9) we only need to show

$$m_{ii} + \theta\Delta t a_{ii} > 0, \quad i = 1, \dots, N_{vi} \quad (27)$$

$$m_{ij} + \theta\Delta t a_{ij} \leq 0 \quad \forall i \neq j, \quad i = 1, \dots, N_{vi}, \quad j = 1, \dots, N_v. \quad (28)$$

Let ω_i be the patch of the elements containing vertex \mathbf{a}_i . Notice that $\nabla\phi_i = 0$ when $K \notin \omega_i$. Recall from [53] that

$$\int_K \phi_i \phi_j d\mathbf{x} = \frac{|K|}{(d+1)(d+2)}, \quad \int_K \phi_i^2 d\mathbf{x} = \frac{2|K|}{(d+1)(d+2)}. \quad (29)$$

Then (27) follows immediately from (10) and Lemma 3.2.

For (28), from (10), (11), and (29) we have

$$\begin{aligned} m_{ij} + \theta\Delta t a_{ij} &= \sum_{K \in \mathcal{T}_h} \int_K \phi_j \phi_i d\mathbf{x} + \theta\Delta t \sum_{K \in \mathcal{T}_h} |K| (\nabla\phi_i)^T \mathbb{D}_K \nabla\phi_j \\ &= \sum_{K \in \omega_i \cap \omega_j} \left(\int_K \phi_j \phi_i d\mathbf{x} + \theta\Delta t |K| (\nabla\phi_i)^T \mathbb{D}_K \nabla\phi_j \right) \\ &= \sum_{K \in \omega_i \cap \omega_j} \left(\int_K \phi_j \phi_i d\mathbf{x} + \theta\Delta t |K| (\nabla\phi_{i_K})^T \mathbb{D}_K \nabla\phi_{j_K} \right), \end{aligned} \quad (30)$$

where i_K and j_K denote the local indices (on element K) of vertices \mathbf{a}_i and \mathbf{a}_j . From (29) and Lemma 3.1, we get

$$m_{ij} + \theta \Delta t a_{ij} = \sum_{K \in \omega_i \cap \omega_j} |K| \left(\frac{1}{(d+1)(d+2)} - \theta \Delta t \frac{\cos(\tilde{\alpha}_{i_K j_K}^K)}{\tilde{h}_{i_K}^K \tilde{h}_{j_K}^K} \right). \quad (31)$$

The right-hand side term is nonpositive if

$$\Delta t \geq \frac{1}{\theta(d+1)(d+2)} \max_{K \in \mathcal{T}_h} \max_{\substack{i,j=1,\dots,d+1 \\ i \neq j}} \frac{\tilde{h}_i^K \tilde{h}_j^K}{\cos(\tilde{\alpha}_{ij}^K)}. \quad (32)$$

Moreover, (21) implies

$$\tilde{h}_i^K = \frac{1}{\|\tilde{\mathbf{q}}_i\|} = \frac{1}{\sqrt{\mathbf{q}_i^T \mathbb{D}_K \mathbf{q}_i}}.$$

Thus, we have

$$\frac{h_i^K}{\sqrt{\lambda_{\max}(\mathbb{D}_K)}} \leq \tilde{h}_i^K \leq \frac{h_i^K}{\sqrt{\lambda_{\min}(\mathbb{D}_K)}}. \quad (33)$$

From this, we can see that (26) implies (32). Hence, we have shown that B is a Z -matrix when (26) holds.

To show B is an M -matrix, we recall from (16) that

$$B = \begin{bmatrix} M_{11} + \theta \Delta t A_{11} & M_{12} + \theta \Delta t A_{12} \\ 0 & I \end{bmatrix}.$$

The fact that B is a Z -matrix means that $M_{11} + \theta \Delta t A_{11}$ is also a Z -matrix and $M_{12} + \theta \Delta t A_{12} \leq 0$. It is easy to show that $M_{11} + \theta \Delta t A_{11}$ is positive definite, which in turn implies $M_{11} + \theta \Delta t A_{11}$ is an M -matrix. Notice

$$B^{-1} = \begin{bmatrix} (M_{11} + \theta \Delta t A_{11})^{-1} & -(M_{11} + \theta \Delta t A_{11})^{-1} (M_{12} + \theta \Delta t A_{12}) \\ 0 & I \end{bmatrix}.$$

This means $B^{-1} \geq 0$ and hence B is an M -matrix. \square

Lemma 3.4. *Matrix C defined in (17) ($0 \leq \theta \leq 1$) is nonnegative if the mesh satisfies (25) and the time step size satisfies*

$$\Delta t \leq \frac{2}{(1-\theta)(d+1)(d+2)} \min_{K \in \mathcal{T}_h} \min_{i=1,\dots,d+1} \frac{(h_i^K)^2}{\lambda_{\max}(\mathbb{D}_K)}. \quad (34)$$

Proof. For off-diagonal entries ($i \neq j$, $i = 1, \dots, N_{vi}$, $j = 1, \dots, N_v$), $m_{ij} - (1-\theta)\Delta t a_{ij}$, are nonnegative since $a_{ij} \leq 0$ under condition (25) (cf. Lemma 3.2) and $m_{ij} \geq 0$ from definition (10). To see if the diagonal entries are also nonnegative, from (10), (11), and (29) we have

$$m_{ii} - (1-\theta)\Delta t a_{ii} = \sum_{K \in \omega_i} |K| \left(\frac{2}{(d+1)(d+2)} - \frac{(1-\theta)\Delta t}{(\tilde{h}_{i_K}^K)^2} \right). \quad (35)$$

The right-hand side term is nonnegative if

$$\Delta t \leq \frac{2}{(1-\theta)(d+1)(d+2)} \min_{K \in \mathcal{T}_h} \min_{i=1,\dots,d+1} (\tilde{h}_i^K)^2.$$

From (33) we see that this condition holds when (34) is satisfied. \square

We are now in a position to prove our first main theoretical result.

Theorem 3.1. *Scheme (15) satisfies a discrete maximum principle if the mesh satisfies the anisotropic nonobtuse angle condition (25) and the time step size satisfies (26) and (34), i.e.,*

$$\begin{aligned} & \frac{1}{\theta(d+1)(d+2)} \max_{K \in \mathcal{T}_h} \max_{\substack{i,j=1,\dots,d+1 \\ i \neq j}} \frac{h_i^K h_j^K}{\cos(\tilde{\alpha}_{ij}^K) \lambda_{\min}(\mathbb{D}_K)} \\ & \leq \Delta t \leq \frac{2}{(1-\theta)(d+1)(d+2)} \min_{K \in \mathcal{T}_h} \min_{i=1,\dots,d+1} \frac{(h_i^K)^2}{\lambda_{\max}(\mathbb{D}_K)}. \end{aligned} \quad (36)$$

Proof. Scheme (15) can be expressed as

$$\mathbb{A}\mathbf{U} = \mathbb{F}, \quad (37)$$

where

$$\mathbb{A} = \begin{bmatrix} I & 0 & & & & \\ -C & B & & & & \\ & -C & B & & & \\ & & \cdots & \cdots & & \\ & & & -C & B & \end{bmatrix}, \quad \mathbf{U} = \begin{bmatrix} \mathbf{u}^0 \\ \mathbf{u}^1 \\ \mathbf{u}^2 \\ \vdots \\ \mathbf{u}^N \end{bmatrix}, \quad \mathbb{F} = \begin{bmatrix} \mathbf{u}_0 \\ \Delta t \mathbf{f}^\theta \\ \Delta t \mathbf{f}^{1+\theta} \\ \vdots \\ \Delta t \mathbf{f}^{N-1+\theta} \end{bmatrix}, \quad (38)$$

and B and C are defined in (17). Scheme (37) satisfies a DMP if coefficient matrix \mathbb{A} is an M -matrix and has nonnegative row sums. From Lemmas 3.3 and 3.4 we know that B is an M -matrix and $C \geq 0$. As a result, \mathbb{A} is a Z -matrix. Moreover, we can show $\mathbb{A}^{-1} \geq 0$. Indeed, from (37) we know that $\mathbf{u}^0 = \mathbf{u}_0$ and thus if $\mathbf{u}_0 \geq 0$, we have $\mathbf{u}^0 \geq 0$. Next, from the scheme we have $\mathbf{u}^1 = B^{-1} \Delta t \mathbf{f}^\theta + B^{-1} C \mathbf{u}^0$. Recall that $C \geq 0$ and B is an M -matrix and thus $B^{-1} \geq 0$. Combining these results, we can conclude that $\mathbf{f}^\theta \geq 0$ implies $\mathbf{u}^1 \geq 0$. Similarly, we can show $\mathbf{u}^n \geq 0$ if $\mathbf{f}^{n-1+\theta} \geq 0$, $n = 2, \dots, N$. Thus, we have shown that $\mathbb{F} \geq 0$ implies $\mathbf{U} \geq 0$. This implies $\mathbb{A}^{-1} \geq 0$ and \mathbb{A} is an M -matrix.

We notice that the sum of each of the second to the last (block) rows is

$$B - C = \begin{bmatrix} \Delta t A_{11} & \Delta t A_{12} \\ 0 & I \end{bmatrix}.$$

Since A has nonnegative row sums (cf. Lemma 3.2), \mathbb{A} has nonnegative row sums. Thus, we have proven that \mathbb{A} is an M -matrix and has nonnegative row sums.

Form [33][Theorem 1], we conclude that the solution of (37) satisfies

$$\max_{i=1,\dots,(N+1)N_v} \mathbb{U}_i = \max \left\{ 0, \max_{i \in S(\mathbb{F}^+)} \mathbb{U}_i \right\}, \quad (39)$$

where $S(\mathbb{F}^+)$ is the set of the indices with $\mathbb{F}_i > 0$. When $f(\mathbf{x}, t) \leq 0$, from (18) we know that $\mathbb{F}_i > 0$ holds only for those indices corresponding to the boundary points on $\partial\Omega_T$. Moreover, from (16), (17), and (38) we see that at the boundary points, \mathbb{U}_i is equal to either the boundary function g or the initial function u_0 . Since a piecewise linear function attains its maximum value at vertices, (39) implies that when $f(\mathbf{x}, t) \leq 0$, the solution of (15) satisfies a DMP

$$\max_{n=0,\dots,N} \max_{\mathbf{x} \in \bar{\Omega}} U^n(\mathbf{x}) = \max \left\{ 0, \max_{n=1,\dots,N} \max_{\mathbf{x} \in \partial\Omega} U^n(\mathbf{x}), \max_{\mathbf{x} \in \bar{\Omega}} U^0(\mathbf{x}) \right\}, \quad (40)$$

where

$$U^n(\mathbf{x}) = \sum_{j=1}^{N_{vi}} u_j^n \phi_j(\mathbf{x}) + \sum_{j=N_{vi}+1}^{N_v} u_j^n \phi_j(\mathbf{x}), \quad n = 0, \dots, N.$$

Hence, we have proven that scheme (15) satisfies DMP. \square

Remark 3.1. Consider a special case with $\mathbb{D} = \alpha I$, where α is a positive constant. It is known (e.g., see Emert and Nelson [54]) that the height (or altitude), volume, and cosine of the dihedral angles of a regular d -dimensional simplex K are given by

$$h_K = e_K \sqrt{\frac{d+1}{2d}}, \quad |K| = \frac{\sqrt{d+1}}{d! \sqrt{2^d}} e_K^d, \quad \cos(\alpha_{ij}^K) = \frac{1}{d}, \quad (41)$$

where e_K is the edge length. Thus, if the elements of \mathcal{T}_h are all regular simplexes, (36) reduces to

$$\frac{\max_{K \in \mathcal{T}_h} e_K^2}{2\theta\alpha(d+2)} \leq \Delta t \leq \frac{\min_{K \in \mathcal{T}_h} e_K^2}{(1-\theta)\alpha d(d+2)}. \quad (42)$$

If further the mesh is uniform (and thus all mesh elements have the same volume and same edge length (e)), the above condition becomes

$$\frac{e^2}{2\theta\alpha(d+2)} \leq \Delta t \leq \frac{e^2}{(1-\theta)\alpha d(d+2)}, \quad (43)$$

which is exactly the result of Theorem 20 of [38] where the maximum principle of linear finite element approximation of isotropic diffusion problems is studied. Interestingly, we can rewrite (43) in terms of the number of the elements, N_e . Indeed, since the mesh is uniform, the elements have a constant volume $|\Omega|/N_e$. From (41), we have

$$e = \sqrt{2} N_e^{-\frac{1}{d}} \left(\frac{|\Omega| d!}{\sqrt{d+1}} \right)^{\frac{1}{d}}.$$

Inserting this into (43), we get

$$\frac{N_e^{-\frac{2}{d}}}{\theta\alpha(d+2)} \left(\frac{|\Omega| d!}{\sqrt{d+1}} \right)^{\frac{2}{d}} \leq \Delta t \leq \frac{2N_e^{-\frac{2}{d}}}{(1-\theta)\alpha d(d+2)} \left(\frac{|\Omega| d!}{\sqrt{d+1}} \right)^{\frac{2}{d}}. \quad (44)$$

\square

Remark 3.2. Another special case is that the mesh is uniform in the metric specified by \mathbb{D}^{-1} . It is known [55] that such a mesh satisfies the so-called alignment and equidistribution conditions

$$\frac{\frac{1}{d} \text{tr}((F'_K)^T \mathbb{D}_K^{-1} F'_K)}{\det((F'_K)^T \mathbb{D}_K^{-1} F'_K)^{\frac{1}{d}}} = 1, \quad \forall K \in \mathcal{T}_h \quad (45)$$

$$|K| \sqrt{\det(\mathbb{D}_K^{-1})} = \frac{\sigma_h}{N_e}, \quad \forall K \in \mathcal{T}_h \quad (46)$$

where $\text{tr}(\cdot)$ and $\det(\cdot)$ denote the trace and determinant of a matrix, F'_K is the Jacobian matrix of the affine mapping F_K from the reference element \hat{K} to element K , and

$$\sigma_h = \sum_{K \in \mathcal{T}_h} |K| \sqrt{\det(\mathbb{D}_K^{-1})}. \quad (47)$$

Geometrically, the alignment condition (45) implies that the element \tilde{K} in Fig. 1 is a regular simplex while the equidistribution condition indicates that all elements have a constant volume σ_h/N_e in the metric \mathbb{D}^{-1} .

For such a mesh, it is more suitable to replace (36) by

$$\begin{aligned} & \frac{1}{\theta(d+1)(d+2)} \max_{K \in \mathcal{T}_h} \max_{\substack{i,j=1,\dots,d+1 \\ i \neq j}} \frac{\tilde{h}_i^K \tilde{h}_j^K}{\cos(\tilde{\alpha}_{ij}^K)} \\ & \leq \Delta t \leq \frac{2}{(1-\theta)(d+1)(d+2)} \min_{K \in \mathcal{T}_h} \min_{i=1,\dots,d+1} (\tilde{h}_i^K)^2. \end{aligned} \quad (48)$$

Using the same procedure as in Remark 3.1 and noticing that \tilde{K} is regular, we can get

$$\frac{N_e^{-\frac{2}{d}}}{\theta(d+2)} \left(\frac{\sigma_h d!}{\sqrt{d+1}} \right)^{\frac{2}{d}} \leq \Delta t \leq \frac{2N_e^{-\frac{2}{d}}}{(1-\theta)d(d+2)} \left(\frac{\sigma_h d!}{\sqrt{d+1}} \right)^{\frac{2}{d}}. \quad (49)$$

Notice that the difference between (44) and (49) lies in that the factor, $|\Omega|/\alpha$, has been replaced by the volume of Ω in the metric \mathbb{D}^{-1} , σ_h . \square

Remark 3.3. It is known [27] that a mesh, generated as a uniform mesh in the metric specified by $M_K = \theta_K \mathbb{D}_K^{-1}$ for all $K \in \mathcal{T}_h$, where θ_K is an arbitrary piecewise constant, scalar function defined on Ω , satisfies the anisotropic nonobtuse angle condition (25). The reader is referred to [27] for more information on the generation of such meshes. \square

The lower bound requirement on Δt in (36) can be avoided by using a lumped mass matrix. In this case, scheme (15) is modified into

$$\begin{aligned} & \left(\begin{bmatrix} \bar{M}_{11} & 0 \\ 0 & I \end{bmatrix} + \theta \Delta t \begin{bmatrix} A_{11} & A_{12} \\ 0 & 0 \end{bmatrix} \right) \mathbf{u}^{n+1} = \\ & \left(\begin{bmatrix} \bar{M}_{11} & 0 \\ 0 & 0 \end{bmatrix} - (1-\theta) \Delta t \begin{bmatrix} A_{11} & A_{12} \\ 0 & 0 \end{bmatrix} \right) \mathbf{u}^n + \Delta t \mathbf{f}^{n+\theta}, \end{aligned} \quad (50)$$

where \bar{M}_{11} is the lumped mass matrix with diagonal entries

$$\bar{m}_{ii} = \sum_{j=1}^{N_v} m_{ij}, \quad i = 1, \dots, N_{vi}.$$

The following theorem can be proven in a similar manner as for Theorem 3.1.

Theorem 3.2. *Scheme (50) with a lumped mass matrix satisfies a discrete maximum principle if the mesh satisfies the anisotropic nonobtuse angle condition (25) and the time step size satisfies*

$$\Delta t \leq \frac{1}{(1-\theta)(d+1)} \min_{K \in \mathcal{T}_h} \min_{i=1,\dots,d+1} \frac{(h_i^K)^2}{\lambda_{\max}(\mathbb{D}_K)}. \quad (51)$$

Remark 3.4. If the mesh is uniform in the metric specified by \mathbb{D}^{-1} , the condition (51) reduces to

$$\Delta t \leq \frac{N_e^{-\frac{2}{d}}}{(1-\theta)d} \left(\frac{\sigma_h d!}{\sqrt{d+1}} \right)^{\frac{2}{d}}, \quad (52)$$

where σ_h is defined in (47). \square

3.2 Two dimensional case: $d = 2$

The results in the previous subsection are valid for all dimensions. However, it is known [23] that a Delaunay-type mesh condition, which is weaker than the nonobtuse angle condition (25), is sufficient for a linear finite element approximation to satisfy DMP in two dimensions for steady-state problems. It is interesting to know if this is also true for time-dependent problems.

Consider an arbitrary interior edge e_{ij} . Denote the two vertices of the edge by \mathbf{a}_i and \mathbf{a}_j and the two elements sharing this common edge by K and K' . Let the local indices of the vertices on K be i_K and j_K . The angle of K opposite e_{ij} is denoted by α_{i_K, j_K}^K (when measured in the Euclidean metric) and by $\tilde{\alpha}_{i_K, j_K}^K$ when measured in the metric \mathbb{D}_K^{-1} . Similarly, we have $\alpha_{i_{K'}, j_{K'}}^{K'}$ and $\tilde{\alpha}_{i_{K'}, j_{K'}}^{K'}$.

Lemma 3.5. *The stiffness matrix A defined in (9) and (11) is an M -matrix and has nonnegative row sums if the mesh satisfies the Delaunay-type mesh condition*

$$\frac{1}{2} \left[\tilde{\alpha}_{i_K, j_K}^K + \operatorname{arccot} \left(\sqrt{\frac{\det(\mathbb{D}_K)}{\det(\mathbb{D}_{K'})}} \cot(\tilde{\alpha}_{i_K, j_K}^K) \right) + \tilde{\alpha}_{i_{K'}, j_{K'}}^{K'} + \operatorname{arccot} \left(\sqrt{\frac{\det(\mathbb{D}_{K'})}{\det(\mathbb{D}_K)}} \cot(\tilde{\alpha}_{i_{K'}, j_{K'}}^{K'}) \right) \right] \leq \pi, \quad \forall \text{ interior edges } e_{ij}. \quad (53)$$

Proof. See [23, Theorem 4.1]. □

Lemma 3.6. *Matrix B defined in (16) ($0 < \theta \leq 1$) is an M -matrix if the mesh satisfies (53) and the time step size satisfies*

$$\Delta t \geq \frac{1}{6\theta} \max_{e_{ij}} \frac{|K| + |K'|}{\sqrt{\det(\mathbb{D}_K)} \cot(\tilde{\alpha}_{i_K, j_K}^K) + \sqrt{\det(\mathbb{D}_{K'})} \cot(\tilde{\alpha}_{i_{K'}, j_{K'}}^{K'})}, \quad (54)$$

where the maximum is taken over all interior edges and K and K' are the two elements sharing the common edge e_{ij} .

Proof. Inequality (54) follows from (24), (29), and (30). □

Lemma 3.7. *Matrix C defined in (17) ($0 < \theta \leq 1$) is nonnegative if the mesh satisfies (53) and the time step size satisfies*

$$\Delta t \leq \frac{1}{6(1-\theta)} \min_i \frac{|\omega_i|}{\sum_{K \in \omega_i} |K| \lambda_{\max}(\mathbb{D}_K) (h_{i_K}^K)^{-2}}, \quad (55)$$

where the minimum is taken over all interior vertices and ω_i is the patch of the elements containing \mathbf{a}_i as its vertex.

Proof. The proof is similar to that of Lemma 3.4. Indeed, Lemma 3.5 implies that the off-diagonal entries of C are nonnegative under condition (53). For diagonal entries, from (35) we get

$$m_{ii} - (1-\theta)\Delta t a_{ii} = \frac{|\omega_i|}{6} - (1-\theta)\Delta t \sum_{K \in \omega_i} \frac{|K|}{(\tilde{h}_{i_K}^K)^2}.$$

From (33), we can see that the right-side term of the above equation is nonnegative when (55) holds. □

Using the above results we can prove the following theorems in a similar manner as for Theorems 3.1 and 3.2.

Theorem 3.3. *In two dimensions, scheme (15) satisfies a discrete maximum principle if the mesh satisfies the Delaunay-type mesh condition (53) and the time step size satisfies (54) and (55), i.e.,*

$$\begin{aligned} \frac{1}{6\theta} \max_{e_{ij}} \frac{|K| + |K'|}{\sqrt{\det(\mathbb{D}_K)} \cot(\tilde{\alpha}_{i_K, j_K}^K) + \sqrt{\det(\mathbb{D}_{K'})} \cot(\tilde{\alpha}_{i_{K'}, j_{K'}}^{K'})} \\ \leq \Delta t \leq \frac{1}{6(1-\theta)} \min_i \frac{|\omega_i|}{\sum_{K \in \omega_i} |K| \lambda_{\max}(\mathbb{D}_K) (h_{i_K}^K)^{-2}}, \end{aligned} \quad (56)$$

where the maximum is taken over all interior edges, K and K' are the two elements sharing the common edge e_{ij} , and the minimum is taken over all interior vertices and ω_i is the patch of the elements containing \mathbf{a}_i as its vertex.

Theorem 3.4. *In two dimensions, scheme (50) with a lumped mass matrix satisfies a discrete maximum principle if the mesh satisfies the Delaunay-type mesh condition (53) and the time step size satisfies*

$$\Delta t \leq \frac{1}{3(1-\theta)} \min_i \frac{|\omega_i|}{\sum_{K \in \omega_i} |K| \lambda_{\max}(\mathbb{D}_K) (h_{i_K}^K)^{-2}}. \quad (57)$$

Remark 3.5. Conditions (56) and (57) (for $d = 2$) reduce to (49) and (52), respectively for a uniform mesh in the metric specified by \mathbb{D}^{-1} but are weaker than conditions (36) and (51) for general meshes. \square

4 Numerical results

In this section we present numerical results obtained for three examples in two dimensions to demonstrate the significance of both mesh conditions (25) and (53) and time step conditions (56) and (57) for DMP satisfaction. Three types of mesh are considered. The first is denoted by Mesh45 where the elements are isosceles right triangles with longest sides in the northeast direction. The second one is denoted by Mesh135 where the elements are isosceles right triangles with longest sides in the northwest direction. Examples of Mesh45 and Mesh135 are shown in Figs. 2(a) and (b). The third type of mesh, denoted by M_{DMP} , is a uniform mesh in the metric $M_{DMP} = \mathbb{D}^{-1}$ which guarantees satisfaction of mesh condition (25) (cf. Remark 3.3).

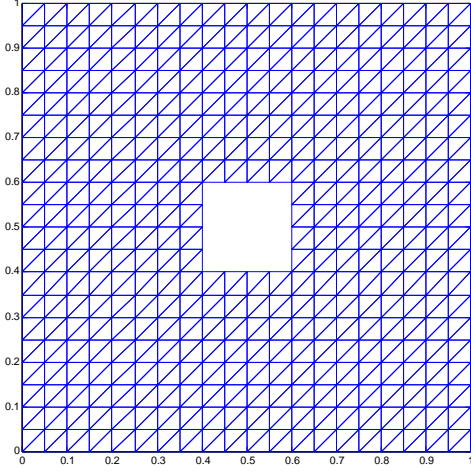
The implicit Euler method (corresponding to $\theta = 1$ in (15)) is used in our computation. For this method, conditions (36), (51), (56), and (57) place no constraint on the upper bound of Δt . For this reason, we consider only the lower bound for the time step size. The lower bound in (36) (related to the anisotropic nonobtuse angle condition) is denoted by Δt_{Ani} and that in (56) (related to the Delaunay-type mesh condition) by Δt_{Del} . Unless stated otherwise, the presented results are obtained after 10 steps of time integration.

Example 4.1. The first example is in the form of IBVP (1) with

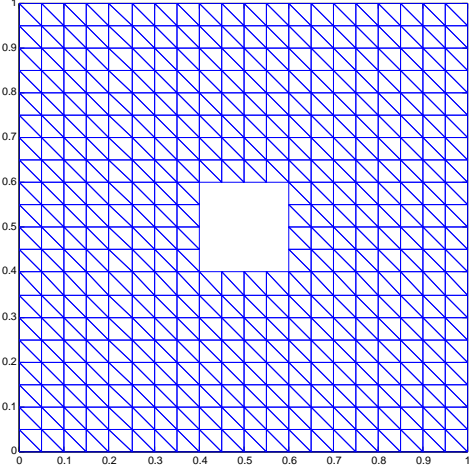
$$f \equiv 0, \quad \Omega = [0, 1]^2 \setminus [0.4, 0.6]^2, \quad g = 0 \text{ on } \Gamma_{out}, \quad g = 4 \text{ on } \Gamma_{in},$$

where Γ_{out} and Γ_{in} are the outer and inner boundaries of Ω , respectively; see Fig. 3(a). The initial solution $u_0(x, y)$ is given as

$$u_0(x, y) = \begin{cases} 4, & \text{on } \Gamma_{in} \\ 0, & \text{in } \Omega \setminus [0.2, 0.8]^2 \\ \text{increases linearly,} & \text{from } \Gamma_{mid} \text{ to } \Gamma_{in} \end{cases}$$



(a): Mesh45



(b): Mesh135

Figure 2: Examples of Mesh45 and Mesh135.

where Γ_{mid} is the boundary of subdomain $[0.2, 0.8]^2$; see Fig. 3. The diffusion matrix is taken as

$$\mathbb{D} = \begin{bmatrix} 50.5 & 49.5 \\ 49.5 & 50.5 \end{bmatrix},$$

which has eigenvalues 100 and 1. The principal eigenvectors are in the northeast direction.

This example satisfies the maximum principle and the exact solution (whose analytical expression is unavailable) stays between 0 and 4. Our goal is to produce a numerical solution which also satisfies DMP and stays between 0 and 4.

We first consider Mesh45 and Mesh135. Mesh45 satisfies the anisotropic nonobtuse angle condition (25) since its maximum angle in the metric $M = \mathbb{D}^{-1}$ is 0.47π . It is known [23] that (25) implies the Delaunay-type mesh condition, (53). By direct calculation we can find that the maximum of the left-hand-side term of (53) is 0.94π . On the other hand, Mesh135 satisfies neither of (25) and (53), with the maximum angle in the metric $M = \mathbb{D}^{-1}$ being 0.94π and the maximum of the left-hand-side term of (53) being 1.87π .

The solution contours (after 10 time steps) using Mesh45 and Mesh135 with $h = 2.5 \times 10^{-2}$ and $\Delta t = 1.5 \times 10^{-4}$ are shown in Fig. 4, where h denotes the maximal height of triangular elements of the mesh and u_{min} is the minimum of the numerical solution. No undershoot occurs in the numerical solution obtained with Mesh45.

The results for Mesh45 are listed in Table 1. They show that for meshes with $h \leq 2.5 \times 10^{-2}$, Δt_{Del} is smaller than the step size $\Delta t = 1.5 \times 10^{-4}$ used in the computation. As a consequence, time condition (56) (and mesh condition (53)) is satisfied and Theorem 3.3 implies that the numerical solution satisfies DMP. Table 1 confirms that no undershoot occurs in the numerical solution or $u_{min} = 0$. On the other hand, for $h = 5.0 \times 10^{-2}$, neither of time conditions (36) and (56) is satisfied and undershoot with $u_{min} = -1.41 \times 10^{-7}$ is observed.

The table also records the numerical results obtained for $h = 2.5 \times 10^{-2}$ and $h = 1.25 \times 10^{-2}$ with decreasing Δt . One can see that no undershoot occurs when $\Delta t \geq \Delta t_{Del}$. However, undershoot occurs when Δt continues to decrease and pass Δt_{Del} . This is consistent with Theorem 3.3.

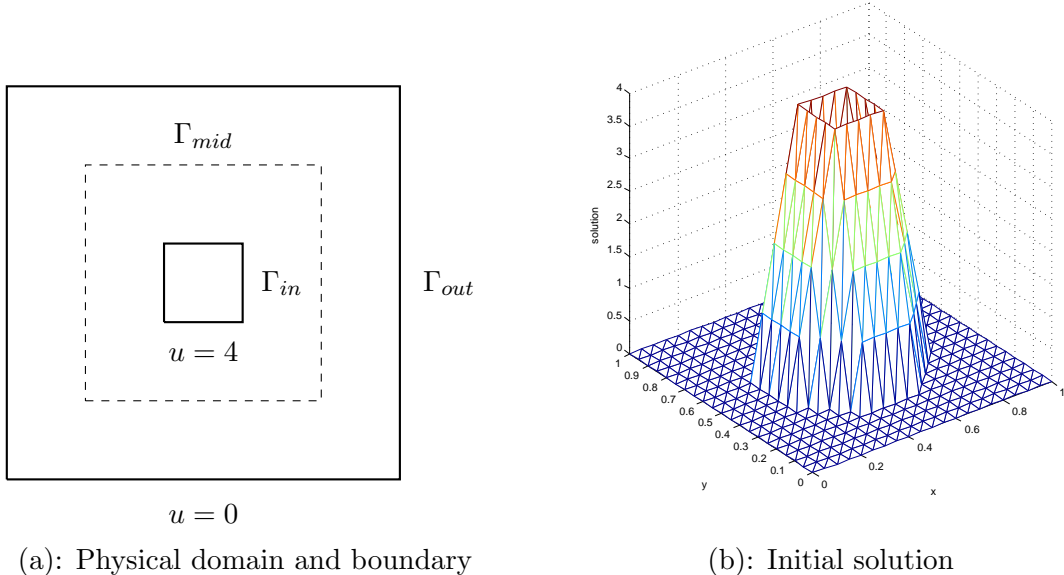


Figure 3: The physical domain, boundary condition, and initial solution for Example 4.1.

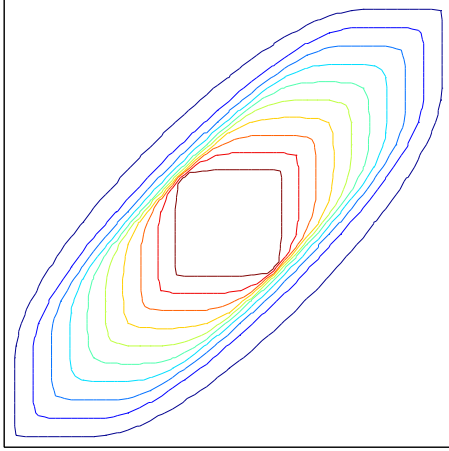
It is pointed out that $\Delta t_{Del} < \Delta t_{Ani}$ for all the cases listed in the table. Moreover, for some cases we have $\Delta t_{Del} < \Delta t < \Delta t_{Ani}$ and no undershoot occurs in the numerical solution. These indicate that time condition (56) (related to the Delaunay-type mesh condition) is weaker than (36) (related to the anisotropic nonobtuse angle condition).

Recall that Mesh135 does not satisfy mesh condition (25) nor (53). Thus, there is no guarantee that the numerical solution obtained with Mesh135 satisfies DMP. Indeed, Table 2 shows that undershoot occurs in all numerical solutions obtained with various sizes of Mesh135 and various Δt .

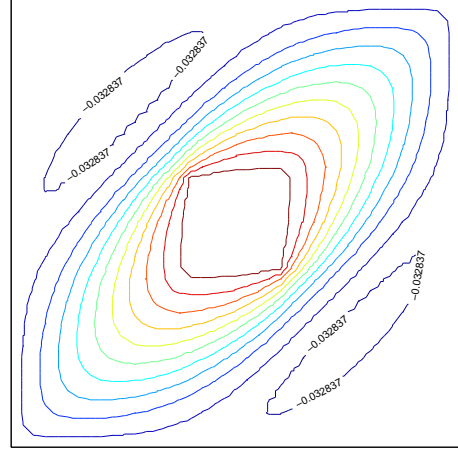
Next we consider M_{DMP} meshes which are generated as (quasi-)uniform ones in the metric specified by $M = \mathbb{D}^{-1}$. Recall from Remark 3.3 that such meshes satisfy the anisotropic nonobtuse angle condition (25). In our computation, M_{DMP} meshes are generated using BAMG (bidimensional anisotropic mesh generator) code developed by Hecht [56]. An example is shown in Fig. 5(b). Notice that the elements are aligned with the principal diffusion direction (northeast). Since the diffusion tensor \mathbb{D} is constant, the mesh is generated initially based on $M_{DMP} = \mathbb{D}^{-1}$ and then kept for the subsequent time steps.

The results obtained with M_{DMP} meshes are similar to those obtained with Mesh45. For example, for the M_{DMP} mesh shown in Fig. 5 (b), it is found numerically that $\Delta t_{Ani} = 4.30 \times 10^{-2}$ and $\Delta t_{Del} = 1.63 \times 10^{-3}$. Theorem 3.3 ensures that no undershoot occurs in the numerical solution when $\Delta t \geq \Delta t_{Del}$. It is emphasized that (53) and (56) are not necessary for DMP satisfaction and the numerical solution may be free of undershoot for some smaller values of Δt . In fact, no undershoot is observed numerically for $\Delta t \geq 10^{-4}$. An undershoot-free solution obtained with the mesh shown in Fig. 5 (b) and time step size $\Delta t = 1.5 \times 10^{-4}$ is shown in Fig. 5 (a). For the same mesh with $\Delta t = 1.0 \times 10^{-5}$, undershoot is observed with $u_{min} = -1.45 \times 10^{-6}$.

Finally, we consider the lumped mass method. Theorem 3.4 implies that there is no constraint placed on Δt for the DMP satisfaction of the numerical solution with the lumped mass matrix and implicit Euler discretization. Indeed, for all Mesh45 meshes and Δt considered in Table 1, no undershoot is observed numerically for the lumped mass method. The same also holds for M_{DMP} meshes. For



(a): Mesh45, $u_{min} = 0$



(b): Mesh135, $u_{min} = -6.57 \times 10^{-2}$

Figure 4: Solution contours obtained for Mesh45 and Mesh135 with $h = 2.5 \times 10^{-2}$ and $\Delta t = 1.5 \times 10^{-4}$ for Example 4.1.

example, for the mesh shown in Fig. 5(b), no undershoot is observed in the numerical solution for $\Delta t = 10^{-4}$, 10^{-5} , and 10^{-6} . For Mesh135 meshes, mesh condition (25) or (53) is not satisfied and thus Theorem 3.4 does not hold. For example, for a case with a Mesh135 mesh with $h = 1.25 \times 10^{-2}$ and $\Delta t = 1.5 \times 10^{-4}$, the numerical solution violates DMP and has a minimum $u_{min} = -1.60 \times 10^{-2}$.

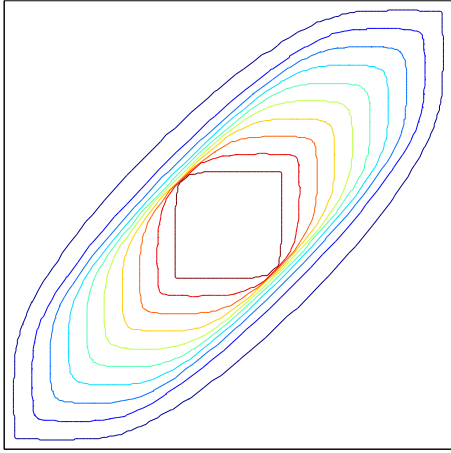
Example 4.2. The second example is the same as Example 4.1 except that the diffusion matrix is taken as a function of x and y , i.e.,

$$\mathbb{D} = \begin{pmatrix} \cos \theta & -\sin \theta \\ \sin \theta & \cos \theta \end{pmatrix} \begin{pmatrix} k_1 & 0 \\ 0 & k_2 \end{pmatrix} \begin{pmatrix} \cos \theta & \sin \theta \\ -\sin \theta & \cos \theta \end{pmatrix}, \quad (58)$$

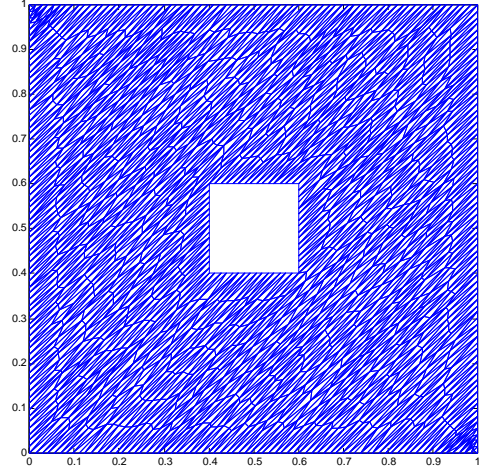
where $k_1 = 100$, $k_2 = 1$, and $\theta = \theta(x, y)$ is the angle of the tangential direction at point (x, y) along circles centered at $(0.5, 0.5)$. This diffusion matrix \mathbb{D} also has eigenvalues 1 and 100 but has its principal eigen-direction along the tangential direction of circles centered at $(0.5, 0.5)$. A physical example with such a diffusion matrix is the toroidal magnetic field in a Tokamak device confining fusion plasma [57]. This problem also satisfies the maximum principle and the solution stays between 0 and 4.

For this example, neither Mesh45 nor Mesh135 (cf. Fig. 2) satisfies the Delaunay-type mesh condition (53). In the metric specified by $M = \mathbb{D}^{-1}$, the maximum of the left-hand side of the inequality is 1.87π for both Mesh45 and Mesh135. Due to the symmetry of the diffusion matrix, both Mesh45 and Mesh135 lead to almost the same results for this example except that undershoot occurs at different locations. Fig. 6 shows the results obtained with these meshes for $\Delta t = 5 \times 10^{-5}$.

Table 3 lists numerical results obtained with Mesh45 and M_{DMP} meshes. Recall that Theorem 3.3 does not apply to Mesh45 meshes since they do not satisfy (53). As a matter of fact, numerical solutions obtained with this type of meshes with or without mass lumping violate DMP and exhibit undershoot. On the other hand, M_{DMP} meshes generated with $M = \mathbb{D}^{-1}$ satisfy the mesh condition. For the lumped mass method, no undershoot occurs in the numerical solution for all values of Δt .



(a): $u_{min} = 0$



(b): M_{DMP} mesh, $N_e = 2362$

Figure 5: An M_{DMP} mesh (with $N_e = 2362$ and $N_v = 1357$) and the corresponding solution obtained with $\Delta t = 1.5 \times 10^{-4}$ for Example 4.1.

This is consistent with Theorem 3.4. For the standard finite element method, there is no undershoot for relatively large Δt . It is interesting to point out that for this example with variable \mathbb{D} , the lower bounds Δt_{Ani} and Δt_{Del} are far too pessimistic. A several magnitude smaller Δt can still lead to numerical solutions free of undershoot.

Example 4.3. This example is the same as the previous examples except that the diffusion matrix is taken as in the form (58) with

$$\theta = \frac{1}{2} \arctan\left(\cos\left(\frac{\pi x}{4}\right)\right), \quad k_1 = 100 \cos\left((x^2 + y^2)\frac{\pi}{6}\right), \quad k_2 = 10 \sin\left((x^2 + y^2 + 1)\frac{\pi}{6}\right).$$

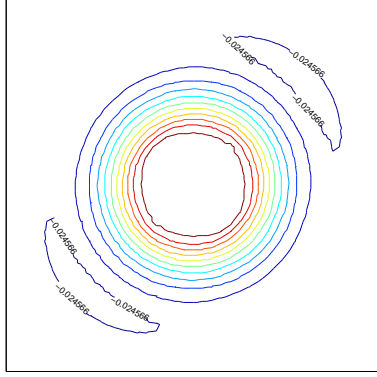
Notice that \mathbb{D} is a function of x and y and both its eigenvalues and eigenvectors vary with location.

Numerical results are shown in Table 4 and Fig. 7. Similar observations can be made as in the previous example. More specifically, both Mesh45 and Mesh135 does not satisfy the Delaunay-type mesh condition (53) and thus there is no guarantee that the obtained numerical solution is undershoot-free. On the other hand, M_{DMP} meshes generated with $M = \mathbb{D}^{-1}$ satisfy (53). The numerical solution is guaranteed to be undershoot-free for sufficiently large Δt for the standard linear finite element method and for all Δt for the lumped mass method.

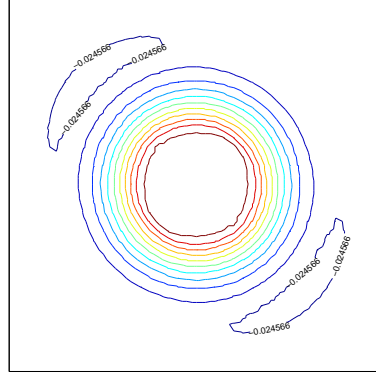
5 Conclusions

In the previous sections we have studied the conditions under which a full discretization for IBVP (1) with a general diffusion matrix function satisfies a discrete maximum principle. The discretization is realized using the θ -method in time and the linear finite element method in space. The main theoretical results are given in Theorems 3.1, 3.2, 3.3, and 3.4.

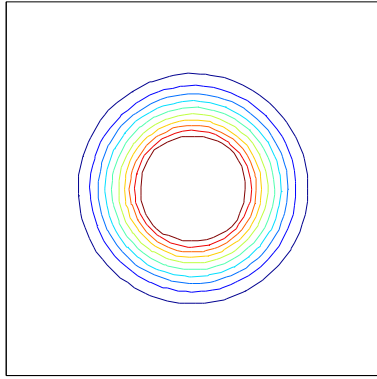
Specifically, the numerical solution obtained with the full discrete scheme satisfies a discrete maximum principle when the mesh satisfies the anisotropic nonobtuse angle condition (25) and the time



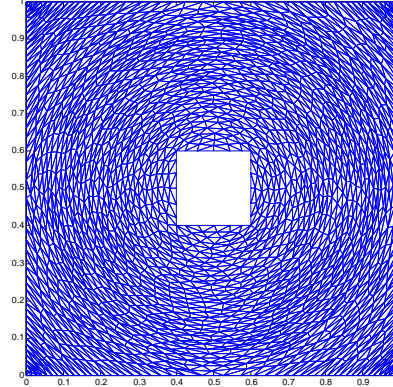
(a): Mesh45, $u_{min} = -4.91 \times 10^{-2}$



(b): Mesh135, $u_{min} = -4.91 \times 10^{-2}$



(c): M_{DMP} , $u_{min} = 0$



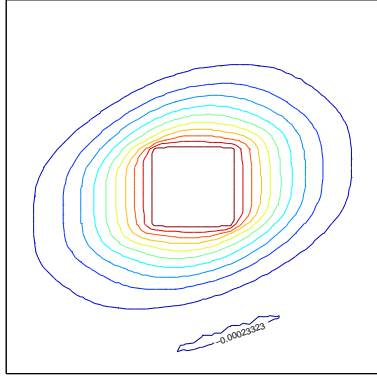
(d): M_{DMP} , $N_e = 3381$

Figure 6: Results obtained with $\Delta t = 5 \times 10^{-5}$ for Example 4.2.

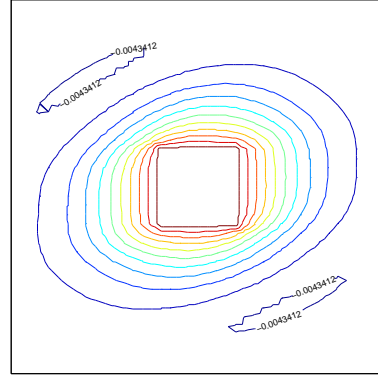
step size satisfies condition (36). As shown in [27], a mesh satisfying (25) can be generated as a uniform mesh in the metric specified by $\alpha \mathbb{D}^{-1}$ with α being a scalar function defined on Ω_T . On the other hand, condition (36) essentially requires the time step size to satisfy

$$C_1 h^2 \leq \Delta t \leq \frac{C_2}{1-\theta} h^2, \quad (59)$$

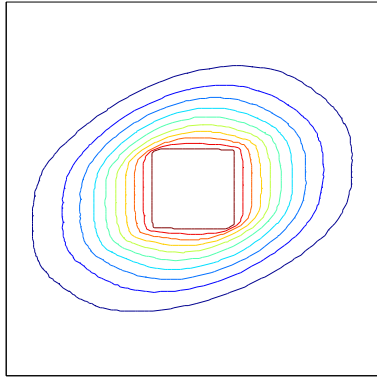
where C_1 and C_2 are positive constants, h is the maximal element diameter, and $\theta \in (0, 1]$ is the parameter used in the θ -method. Obviously, this condition is restrictive. This is especially true when the numerical scheme with $\theta \in [0.5, 1]$ is known to be unconditionally stable and no constraint is placed on Δt for the sake of stability. Moreover, the presence of the lower bound for Δt and the numerical results showing the violation of the maximum principle as $\Delta t \rightarrow 0$ seem to support the finding of Thomée and Wahlbin [48] that a semi-discrete standard Galerkin finite element solution violates DMP since the semi-discrete scheme can be considered as the limit of the full discrete scheme as $\Delta t \rightarrow 0$. Furthermore, Theorems 3.2 and 3.4 show that the lower bound requirement on Δt can be removed when a lumped mass matrix is used. Finally, in two dimensions, the mesh and time step



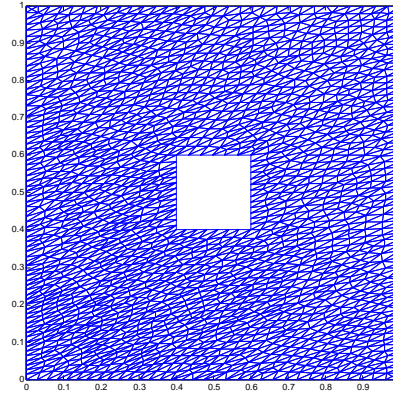
(a): Mesh45, $u_{min} = -4.66 \times 10^{-4}$



(b): Mesh135, $u_{min} = -8.68 \times 10^{-3}$



(c): M_{DMP} , $u_{min} = 0$



(d): M_{DMP} , $N_e = 3180$

Figure 7: Results obtained with $\Delta t = 1 \times 10^{-5}$ for Example 4.3.

conditions can be replaced with weaker conditions (53) and (56), respectively. Numerical results in Sect. 4 confirm the theoretical findings.

Acknowledgment. This work was supported in part by NSF under grant DMS-1115118.

References

- [1] P. E. Farrell, M. D. Piggott, C. C. Pain, G. J. Gorman, and C. R. Wilson. Conservative interpolation between unstructured meshes via supermesh construction. *Comput. Methods Appl. Mech. Engrg.* 198:2632–2642, 2009.
- [2] S. Günter and K. Lackner. A mixed implicit-explicit finite difference scheme for heat transport in magnetised plasmas. *J. Comput. Phys.*, 228:282–293, 2009.

- [3] S. Günter, K. Lackner, and C. Tichmann. Finite element and higher order difference formulations for modelling heat transport in magnetised plasmas. *J. Comput. Phys.*, 226:2306–2316, 2007.
- [4] S. Günter, Q. Yu, J. Kruger, and K. Lackner. Modelling of heat transport in magnetised plasmas using non-aligned coordinates. *J. Comput. Phys.*, 209:354–370, 2005.
- [5] K. Nishikawa and M. Wakatani. *Plasma Physics*. Springer-Verlag Berlin Heidelberg, New York, 2000.
- [6] P. Sharma and G. W. Hammett. Preserving monotonicity in anisotropic diffusion. *J. Comput. Phys.*, 227:123–142, 2007.
- [7] T. Stix. *Waves in Plasmas*. Amer. Inst. Phys., New York, 1992.
- [8] I. Aavatsmark, T. Barkve, Ø. Bøe, and T. Mannseth. Discretization on unstructured grids for inhomogeneous, anisotropic media. I. Derivation of the methods. *SIAM J. Sci. Comput.*, 19:1700–1716 (electronic), 1998.
- [9] I. Aavatsmark, T. Barkve, Ø. Bøe, and T. Mannseth. Discretization on unstructured grids for inhomogeneous, anisotropic media. II. Discussion and numerical results. *SIAM J. Sci. Comput.*, 19:1717–1736 (electronic), 1998.
- [10] P. I. Crumpton, G. J. Shaw, and A. F. Ware. Discretisation and multigrid solution of elliptic equations with mixed derivative terms and strongly discontinuous coefficients. *J. Comput. Phys.*, 116:343–358, 1995.
- [11] T. Ertekin, J. H. Abou-Kassem, and G. R. King. *Basic Applied Reservoir Simulation*. SPE textbook series, Vol. 7, Richardson, Texas, 2001.
- [12] M. J. Mlacnik and L. J. Durlofsky. Unstructured grid optimization for improved monotonicity of discrete solutions of elliptic equations with highly anisotropic coefficients. *J. Comput. Phys.*, 216:337–361, 2006.
- [13] T. F. Chan and J. Shen. Non-texture inpainting by curvature driven diffusions (CDD). *J. Vis. Commun. Image Rep*, 12:436–449, 2000.
- [14] T. F. Chan, J. Shen, and L. Vese. Variational PDE models in image processing. *Not. AMS J.*, 50:14–26, 2003.
- [15] D. A. Karras and G. B. Mertzios. New PDE-based methods for image enhancement using SOM and Bayesian inference in various discretization schemes. *Meas. Sci. Technol.*, 20:104012, 2009.
- [16] D. Mumford and J. Shah. Optimal approximations by piecewise smooth functions and associated variational problems. *Commun. Pure Appl. Math*, 42:577–685, 1989.
- [17] P. Perona and J. Malik. Scale-space and edge detection using anisotropic diffusion. *IEEE Trans. Pattern Anal. Mach. Intel.*, 12:629–639, 1990.
- [18] J. Weickert. *Anisotropic Diffusion in Image Processing*. Teubner-Verlag, Stuttgart, Germany, 1998.

- [19] J. Brandts, S. Korotov, and M. Křížek. The discrete maximum principle for linear simplicial finite element approximations of a reaction-diffusion problem. *Lin. Alg. Appl.*, 429:2344–2357, 2008.
- [20] P. G. Ciarlet. Discrete maximum principle for finite difference operators. *Aequationes Math.*, 4:338–352, 1970.
- [21] P. G. Ciarlet and P.-A. Raviart. Maximum principle and uniform convergence for the finite element method. *Comput. Meth. Appl. Mech. Engrg.*, 2:17–31, 1973.
- [22] A. Drăgănescu, T. F. Dupont, and L. R. Scott. Failure of the discrete maximum principle for an elliptic finite element problem. *Math. Comp.*, 74:1–23, 2004.
- [23] W. Huang. Discrete maximum principle and a delaunay-type mesh condition for linear finite element approximations of two-dimensional anisotropic diffusion problems. *Numer. Math. Theory Meth. Appl.*, 4:319–334, 2011. (arXiv:1008.0562v1).
- [24] J. Karátson and S. Korotov. Discrete maximum principles for finite element solutions of nonlinear elliptic problems with mixed boundary conditions. *Numer. Math.*, 99:669–698, 2005.
- [25] J. Karátson, S. Korotov, and M. Křížek. On discrete maximum principles for nonlinear elliptic problems. *Math. Comput. Sim.*, 76:99–108, 2007.
- [26] D. Kuzmin, M. J. Shashkov, and D. Svyatskiy. A constrained finite element method satisfying the discrete maximum principle for anisotropic diffusion problems. *J. Comput. Phys.*, 228:3448–3463, 2009.
- [27] X. P. Li and W. Huang. An anisotropic mesh adaptation method for the finite element solution of heterogeneous anisotropic diffusion problems. *J. Comput. Phys.*, 229:8072–8094, 2010 (arXiv:1003.4530v2).
- [28] X. P. Li, D. Svyatskiy, and M. Shashkov. Mesh adaptation and discrete maximum principle for 2D anisotropic diffusion problems. Technical Report LA-UR 10-01227, Los Alamos National Laboratory, Los Alamos, NM, 2007.
- [29] R. Liska and M. Shashkov. Enforcing the discrete maximum principle for linear finite element solutions of second-order elliptic problems. *Comm. Comput. Phys.*, 3:852–877, 2008.
- [30] C. Lu, W. Huang, and J. Qiu. Maximum principle in linear finite element approximations of anisotropic diffusion-convection-reaction problems. (*submitted*), 2012 (arXiv:1201.3564v1).
- [31] Z. Sheng and G. Yuan. The finite volume scheme preserving extremum principle for diffusion equations on polygonal meshes. *J. Comput. Phys.*, 230:2588–2604, 2011.
- [32] G. Stoyan. On a maximum principle for matrices, and on conservation of monotonicity. With applications to discretization methods. *Z. Angew. Math. Mech.*, 62:375–381, 1982.
- [33] G. Stoyan. On maximum principles for monotone matrices. *Lin. Alg. Appl.*, 78:147–161, 1986.
- [34] G. Strang and G. J. Fix. *An Analysis of the Finite Element Method*. Prentice Hall, Englewood Cliffs, NJ, 1973.

- [35] J. Wang and R. Zhang. Maximum principle for P1-conforming finite element approximations of quasi-linear second order elliptic equations. 2011. (arXiv:1105.1466v3).
- [36] C. Yuan and Z. Sheng. Monotone finite volume schemes for diffusion equations on polygonal meshes. *J. Comput. Phys.*, 227:6288–6312, 2008.
- [37] L. Dascal. Well-posedness and maximum principle for PDE based models in image processing. PhD thesis, Tel-Aviv University, 2006.
- [38] I. Faragó. Discrete maximum principle for finite element parabolic models in higher dimensions. *Math. Comput. Simulation*, 80:1601–1611, 2010.
- [39] I. Faragó and R. Horváth. Discrete maximum principle and adequate discretizations of linear parabolic problems. *SIAM J. Sci. Comput.*, 28:2313–2336, 2006.
- [40] I. Faragó and R. Horváth. A review of reliable numerical models for three-dimensional linear parabolic problems. *Int. J. Numer. Meth. Engng.*, 70:25–45, 2007.
- [41] I. Faragó and R. Horváth. Continuous and discrete parabolic operators and their qualitative properties. *IMA J. Numer. Anal.*, 29:606–631, 2009.
- [42] I. Faragó, R. Horváth, and S. Korotov. Discrete maximum principle for linear parabolic problems solved on hybrid meshes. *Appl. Numer. Math.*, 53:249–264, 2005.
- [43] I. Faragó, Karátson, and S. Korotov. Discrete maximum principles for nonlinear parabolic pde systems. Technical Report 93, Tampere University of Technology. Department of Mathematics, 2009.
- [44] H. Fujii. Some remarks on finite element analysis of time-dependent field problems. In *Theory and Proactice in Finite Element Structural Analysis*, pages 91–106. University of Tokyo, Tokyo, 1973.
- [45] I. Harari. Stability of semidiscrete formulations for parabolic problems at small time steps. *Comput. Methods Appl. Mech. Engrg.*, 193:1491–1516, 2004.
- [46] M. Lobo and A. F. Emery. The discrete maximum principle in finite-element thermal radiation analysis. *Numer. Heat Transfer, Part B*, 24:209–227, 1993.
- [47] V. Murti, S. Valliappan, and N. Khalili-Naghadeh. Time step constraints in finite element analysis of the poisson type equations. *Comput. Struct.*, 31:269–273, 1989.
- [48] V. Thomée and L. B. Wahlbin. On the existence of maximum principles in parabolic finite element equations. *Math. Comput.*, 77:11–19, 2008.
- [49] T. Vejchodský, S. Korotov, and A. Hannukainen. Discrete maximum principle for parabolic problems solved by prismatic finite elements. Technical Report 77, Institute of Mathematics, AS CR, Prague, 2008.
- [50] C. Yang and Y. Gu. Minimum time-step criteria for the galerkin finite element methods applied to one-dimensional parabolic partial differential equations. *Numer Meth. P. D. E.*, 22:259–273, 2006.

- [51] C. Le Potier. Schéma volumes finis monotone pour des opérateurs de diffusion fortement anisotropes sur des maillages de triangles non structurés. *C. R. Math. Acad. Sci. Paris*, 341:787–792, 2005.
- [52] C. Le Potier. A nonlinear finite volume scheme satisfying maximum and minimum principles for diffusion operators. *Int. J. Finite Vol.*, 6(2):20 pp, 2009.
- [53] P. G. Ciarlet. *The Finite Element Method for Elliptic Problems*. North-Holland, Amsterdam, 1978.
- [54] J. Emert and R. Nelson. Volume and Surface Area for Polyhedra and Polytopes. *Math. Mag.* 70:365–371, 1997.
- [55] W. Huang and R. D. Russell. *Adaptive Moving Mesh Methods*. Springer-Verlag Berlin Heidelberg, New York, 2011.
- [56] F. Hecht. BAMG – Bidimensional Anisotropic Mesh Generator homepage. <http://www.ann.jussieu.fr/~hecht/ftp/bamg/>, 1997.
- [57] A. R. Sanderson, G. Chen, X. Tricoche, D. Pugmire, S. Kruger, and J. Breslau. Analysis of recurrent patterns in toroidal magnetic fields. *IEEE Trans. Vis. Comput. Graph.*, 16:1431–1440, 2010.

List of Figures

Figure 1: Sketch of coordinate transformations from \hat{K} to K and to \tilde{K} .

Figure 2: Examples of Mesh45 and Mesh135.

Figure 3: The physical domain, boundary condition, and initial solution for Example 4.1.

Figure 4: Solution contours obtained for Mesh45 and Mesh135 with $h = 2.5 \times 10^{-2}$ and $\Delta t = 1.5 \times 10^{-4}$ for Example 4.1.

Figure 5: An M_{DMP} mesh (with $N_e = 2362$ and $N_v = 1357$) and the corresponding solution obtained with $\Delta t = 1.5 \times 10^{-4}$ for Example 4.1.

Figure 6: Results obtained with $\Delta t = 5 \times 10^{-5}$ for Example 4.2.

Figure 7: Results obtained with $\Delta t = 1 \times 10^{-5}$ for Example 4.3.

Tables

Table 1: Numerical results obtained with Mesh45 for Example 4.1.

h	Δt_{Ani}	Δt_{Del}	Δt	u_{min}
5.0e-2	1.48e-3	3.79e-4	1.5e-4	-1.41e-7
2.5e-2	3.70e-4	9.47e-5	1.5e-4	0
1.25e-2	9.25e-5	2.37e-5	1.5e-4	0
6.25e-3	2.31e-5	5.92e-6	1.5e-4	0
3.125e-3	5.78e-6	1.48e-6	1.5e-4	0
2.5e-2	3.70e-4	9.47e-5	1.5e-4	0
2.5e-2	3.70e-4	9.47e-5	1.0e-4	0
2.5e-2	3.70e-4	9.47e-5	5.0e-5	-7.91e-10
1.25e-2	9.25e-5	2.37e-5	1.5e-4	0
1.25e-2	9.25e-5	2.37e-5	1.0e-5	-1.31e-6

Table 2: Numerical results obtained with Mesh135 for Example 4.1.

h	Δt_{Ani}	Δt_{Del}	Δt	u_{min}
5.0e-2	1.48e-4	2.08e-6	1.5e-4	-8.99e-2
2.5e-2	3.70e-5	5.21e-7	1.5e-4	-6.57e-2
1.25e-2	9.25e-6	1.30e-7	1.5e-4	-1.58e-2
1.25e-2	9.25e-6	1.30e-7	1.0e-7	-2.26e-2
6.25e-3	2.31e-6	3.26e-8	5.0e-4	-1.59e-3
6.25e-3	2.31e-6	3.26e-8	1.5e-5	-1.43e-2
6.25e-3	2.31e-6	3.26e-8	1.5e-6	-2.11e-2

Table 3: Results obtained with Mesh45 and M_{DMP} meshes for Example 4.2.

Mesh	N_e	Δt_{Ani}	Δt_{Del}	Δt	u_{min}	u_{min} (lumped mass)
Mesh45	3072	3.47e-4	1.17e-2	1.0e-4	-4.31e-2	-4.11e-2
				5.0e-5	-4.91e-2	-4.78e-2
				2.0e-5	-5.49e-2	-5.36e-2
				1.0e-5	-5.70e-2	-5.26e-2
M_{DMP}	3381	8.61e-2	3.06e-2	5.0e-2	0	0
				1.0e-4	0	0
				5.0e-5	0	0
				2.0e-5	-1.20e-5	0
				1.0e-5	-5.02e-4	0

Table 4: Results obtained with M_{DMP} meshes for Example 4.3.

N_e	Δt_{Ani}	Δt_{Del}	Δt	u_{min}	u_{min} (lumped mass)
3180	1.83e-2	6.38e-4	1.0e-4	0	0
			5.0e-5	0	0
			1.0e-5	0	0
			2.5e-6	-7.67e-5	0
			1.0e-6	-6.21e-3	0